



## Comparative analysis of single and two-phase models for CFD studies of nanofluid heat transfer

M. Akbari<sup>a,\*</sup>, N. Galanis<sup>a</sup>, A. Behzadmehr<sup>b</sup>

<sup>a</sup> *Faculté de génie, Université de Sherbrooke, Sherbrooke, Quebec, Canada J1K 2R1*

<sup>b</sup> *Mechanical Engineering, University of Sistan and Baluchestan, Zahedan, Sistan and Baluchestan, Iran*

### ARTICLE INFO

#### Article history:

Received 17 November 2010

Accepted 8 March 2011

Available online 12 April 2011

#### Keywords:

Nanofluids

Mixed convection

CFD

Single-phase model

Two-phase models

### ABSTRACT

CFD predictions of laminar mixed convection of  $\text{Al}_2\text{O}_3$ –water nanofluids by single-phase and three different two-phase models (volume of fluid, mixture, Eulerian) are compared. The elliptical, coupled, steady-state, three-dimensional governing partial differential equations for laminar mixed convection in a horizontal tube with uniform heat flux are solved numerically using the finite volume approach. It is found that single-phase and two-phase models predict almost identical hydrodynamic fields but very different thermal ones. The predictions by the three two-phase models are essentially the same. For the problem under consideration the two-phase models give closer predictions of the convective heat transfer coefficient to the experimental data than the single-phase model; nevertheless, the two-phase models over-predict the enhancement of the convective heat transfer coefficient resulting from the increase of the alumina volume fraction. The results are calculated for two Reynolds numbers (1050 and 1600) and three nanoparticle volume concentrations (<2%). Although single-phase and two-phase models have been used before to analyze mixed convection of nanofluids, this is the first systematic comparison of their predictions for a laminar mixed convection flow which includes the hydrodynamic characteristics and the effect of temperature dependent properties.

© 2011 Elsevier Masson SAS. All rights reserved.

### 1. Introduction

The low conductivity of liquids such as water, ethylene glycol, and engine oil which are used as heat transfer fluids in many industrial and residential applications constitutes an important drawback which limits the performance of engineering equipments such as heat exchangers and electronic devices. There has been a serious effort to overcome this problem since Maxwell [1] investigated the possibility of increasing the thermal performance of ordinary fluids by adding solid particles. Maxwell's study showed that the conductivity of liquid–solid mixtures improves with increasing particle volume fraction. This was the first step of an innovative approach aiming to improve the conductivity of liquids by adding small particles into the fluids. At first, millimetre or micrometer size particles were used which have a high risk of sedimentation and can cause erosion as well as high pressure loss. Later, technological progress led to the fabrication of nanosized particles which mix homogeneously with the base fluid, remain in suspension for long periods, and have a high thermal conductivity

even for very small particle volume fractions. Compared with other techniques for heat transfer enhancement, these nanofluids (a name first proposed by Choi [2]) show considerable potential as replacements of conventional heat transfer fluids.

For heat transfer in ducts, buoyancy forces have a significant effect on the hydrodynamic and thermal fields, particularly for laminar flow in horizontal ducts. They generate secondary flows which lead to Nusselt numbers and friction coefficients very different from those corresponding to forced convection. In the case of conventional heat transfer fluids, these phenomena have been studied extensively [3–8]. In the case of nanofluids, some numerical studies of laminar mixed convection inside horizontal and inclined tubes considered the nanofluids as single-phase homogeneous mixtures [9,10], while others have used the two-phase approach [11,12]. However, none of them includes a systematic comparison of two phase and single phase mixed convection predictions.

Lotfi et al. [13] have compared the single-phase with the Mixture and Eulerian two-phase models for the forced convection flow of  $\text{Al}_2\text{O}_3$ –Water nanofluid with temperature independent properties. Specifically, they have compared the Nusselt number predictions for a 1% value concentration of nanoparticles with several correlations and one set of experimental values. They have also considered the effect of volume concentration on the wall

\* Corresponding author.

E-mail address: [Mahmood.Akbari@usherbrooke.ca](mailto:Mahmood.Akbari@usherbrooke.ca) (M. Akbari).

Nomenclature		$v$	Radial Velocity Component
$C_p$	Specific Heat	$w$	Axial Velocity Component
$\bar{C}_{R.M.}$	Nanoparticles Random Motion Velocity	$Z$	Axial Direction
$D$	Tube Diameter	<i>Greek Letters</i>	
$D_o$	Diffusion Coefficient	$\beta$	Thermal Expansion Coefficient
$d_f$	Liquid Layer Thickness	$\theta$	Angular Direction
$d_s$	Particle Diameter	$\varphi$	Volume Fraction
$g$	Gravitational Acceleration	$\mu$	Dynamic Viscosity
$H$	Entropy	$\nu$	Kinematic Viscosity
$h$	Convective Heat Transfer Coefficient	$\rho$	Density
$K$	Conductivity	$\tau$	Stress–Strain Tensor
$k_b$	Boltzmann's Constant	<i>Subscripts</i>	
$L$	Tube Length	<i>eff</i>	Effective
$l$	Mean Free Path	<i>f</i>	Base Fluid
$P$	Pressure	<i>in</i>	Inlet
$q$	Heat Flux	<i>m</i>	Mixture
$R$	Tube Radius	<i>nf</i>	Nanofluid
$r$	Radial Direction	<i>s</i>	Solid Particle
$T$	Temperature	<i>w</i>	Wall
$u$	Angular Velocity Component		
$V$	Velocity		

temperature. They concluded that the Mixture model is more precise than the other two models.

The present study was therefore undertaken to examine whether the conclusions of Lotfi et al. [13] are also valid in the case of mixed convection. For this purpose, the single phase (homogeneous mixture) and three different two-phase models (Volume of fluid, Mixture and Eulerian) are used to analyze laminar mixed convection flow of a water–Al<sub>2</sub>O<sub>3</sub> nanofluid in a horizontal tube with uniform heat flux applied at the nanofluid–solid interface. All the fluid properties are considered to be temperature dependent. The numerical predictions of the convective heat transfer coefficient are compared with published experimental data [14] in order to evaluate the accuracy of each of these four models. Their predictions of the velocity and temperature fields for three nanoparticle concentrations are then compared in order to analyze their similarities and differences.

## 2. Description and modeling of the problem

Laminar mixed convection of a nanofluid consisting of water and Al<sub>2</sub>O<sub>3</sub> nanoparticles ( $d_s = 42$  nm) in a long horizontal tube ( $D = 0.0045$  m,  $L = 0.97$  m) with uniform heat flux at the solid–liquid interface is considered (Fig. 1). The physical properties of the base fluid are considered to be temperature dependent while those of the solid particles are constant. Material property correlations and the differential equations for the three two-phase models and the single-phase model are presented in the following sections.

### 2.1. Water properties

The following equations for water properties are used in all four models under consideration.

- Density [15]:

$$\rho_f = 2446 - 20.674T + 0.11576T^2 - 3.12895 \times 10^{-4}T^3 + 4.0505 \times 10^{-7}T^4 - 2.0546 \times 10^{-10}T^5 \quad (1)$$

- Viscosity [16]:

$$\mu_f = A10 \left( \frac{B}{T - C} \right) \quad (2)$$

where,  $A = 2.414 \times 10^{-5}$ ,  $B = 247.8$ , and  $C = 140$ .

- Specific heat [15]

$$(C_p)_f = \exp \left( \frac{8.29041 - 0.012557T}{1 - (1.52373 \times 10^{-3})T} \right) \quad (3)$$

### 2.2. Single-phase model

This model treats the nanofluid as a homogeneous fluid with effective properties and uses the differential equations expressing conservation of mass, momentum, and energy. To obtain accurate results with the single-phase model, it is very important to use the most appropriate correlations for the effective nanofluid properties.

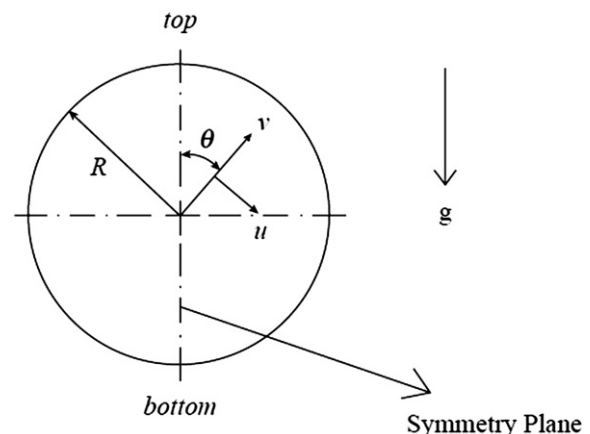


Fig. 1. Cross section of the horizontal tube and coordinate system.

Up to now, however, there are no universal correlations that can accurately predict nanofluid properties for any combination of independent variables (nature of particles, diameter of particles, etc.). Many different correlations available in the literature lead to contradictory results [17] and it is not clear which one is best for a given situation. Nevertheless, all sources indicate that the nanofluid properties depend on the volume fraction of particles as well as on the corresponding properties of the base fluid and the solid particles. Since the properties of the base fluid are temperature dependent, those of the nanofluid are also temperature dependent. Consequently, in this study all the nanofluid properties are expressed as functions of the volume fraction and the temperature as follows:

- Density [18]

$$\rho_{nf} = (1 - \varphi)\rho_f + \varphi\rho_s \quad (4)$$

- Viscosity [19]

$$\mu_{nf} = (1 + 0.025\varphi + 0.015\varphi^2)\mu_f \quad (5)$$

- Conductivity [20]

$$K_{nf} = K_f(1 - \varphi) + \gamma K_s\varphi + C_d \frac{d_f}{d_s} K_f Re_s^2 Pr\varphi \quad (6)$$

where  $\gamma = 0.01$  (a constant taking into account the Kapitza resistance per unit area),  $C_d = 18 \times 10^{-6}$  (a constant) and:

$$Re_s = \left( \frac{\bar{C}_{R.M.} d_s}{\nu} \right) \quad (7)$$

For the present calculation a constant value equal to 0.1 m/s has been used for the random motion velocity  $C_{R.M.}$  as recommended by Jang and Choi [20].

- Specific heat [18]

$$(C_p)_{nf} = \frac{(1 - \varphi)(\rho C_p)_f + \varphi(\rho C_p)_s}{\rho_{nf}} \quad (8)$$

The differential equations for this model (conservation of mass, momentum and energy) are:

$$\nabla \cdot (\rho \vec{V}) = 0 \quad (9)$$

$$\rho \vec{V} \cdot \nabla \vec{V} = -\nabla P + \nabla \cdot (\mu \nabla \vec{V}) + \rho g \quad (10)$$

$$\rho \nabla \cdot (\vec{V} H) = -\nabla \cdot q - \tau : \nabla \vec{V} \quad (11)$$

All the nanofluids properties are temperature dependent. Since the density is temperature dependent the buoyancy induced secondary flows are included in the calculations.

### 2.3. Two-phase models

There are two general approaches for modeling the flow of solid-liquid mixtures. For low solid volume fractions, the most suitable approach is the Lagrangian–Eulerian which analyzes the base fluid by the Eulerian assumption and the particle phase by the Lagrangian one. For higher solid volume fractions, the appropriate approach is the Eulerian–Eulerian. For nanofluids, the number of particles in the computational domain, even for a very small particle volume

fraction, is extremely large due to the very small size of the particles. This makes it impossible to solve the nanofluid flow problems by the Lagrangian–Eulerian approach due to limitations of the software abilities, memory and CPU requirements, etc. Therefore, the Eulerian–Eulerian approach is used in the present study. In fact, there are different Eulerian–Eulerian models. The most popular ones are the VOF (volume of fluid), mixture, and Eulerian.

#### 2.3.1. VOF

The VOF model solves a single set of momentum equations for all the phases and tracks their volume fraction all over the domain of study by solving a continuity equation for the secondary phases. The total summation of the volume fractions for all the phases is equal to unity. Therefore, the magnitude of the primary phase volume fraction will be calculated. In this method, all of the physical properties are calculated by taking a weighted average of different phases based on their volume fraction throughout each control volume. The single set of momentum equation is solved to find the velocity components, which are shared by all the phases. In the same manner, a shared temperature is calculated from a single energy equation. Specifically, mass conservation is expressed as

$$\nabla \cdot (\varphi_q \rho_q \vec{V}_q) = 0 \quad (12)$$

where  $\sum_{q=1}^n \varphi_q = 1$  and all properties are calculated like  $N = \sum_{q=1}^n \varphi_q N_q$ .

The conservation of momentum and energy equations are identical to Eqs. (10) and (11).

#### 2.3.2. Mixture

The mixture model solves the continuity, momentum and energy equations for the mixture as well as a volume fraction equation for the secondary phases. It then uses a correlation to calculate the relative velocity between the phases. The relevant equations are:

- Conservation of mass

$$\nabla \cdot (\rho_m \vec{V}_m) = 0 \quad (13)$$

- Conservation of momentum

$$\rho_m \vec{V}_m \cdot \nabla \vec{V}_m = -\nabla P_m + \nabla \cdot (\mu_m \nabla \vec{V}_m) + \rho_m g + \nabla \cdot \left( \sum_{k=1}^n \varphi_k \rho_k \vec{V}_{dr,k} \vec{V}_{dr,k} \right) \quad (14)$$

where the mixture velocity, density and viscosity are respectively

$$\vec{V}_m = \frac{\sum_{k=1}^n \varphi_k \rho_k \vec{V}_k}{\rho_m} \quad (15)$$

$$\rho_m = \sum_{k=1}^n \varphi_k \rho_k \quad (16)$$

$$\mu_m = \sum_{k=1}^n \varphi_k \mu_k \quad (17)$$

The drift velocity of  $k^{\text{th}}$  phase is

$$\vec{V}_{dr,k} = \vec{V}_k - \vec{V}_m \quad (18)$$

- Conservation of energy

$$\nabla \cdot \left( \sum_{k=1}^n \varphi_k \rho_k \vec{V}_k H_k \right) = -\nabla \cdot q_m - \tau_m : \nabla \vec{V}_m \quad (19)$$

- Volume Fraction

$$\nabla \cdot (\varphi_p \rho_p \vec{V}_m) = -\nabla \cdot (\varphi_p \rho_p \vec{V}_{dr,p}) \quad (20)$$

The slip velocity (relative velocity) is defined as the velocity of a secondary phase ( $p$ ) relative to the velocity of the primary phase ( $f$ ):

$$\vec{V}_{pf} = \vec{V}_p - \vec{V}_f \quad (21)$$

The drift velocity is related to the relative velocity as:

$$\vec{V}_{dr,p} = \vec{V}_{pf} - \sum_{k=1}^n \frac{\varphi_k \rho_k}{\rho_{eff}} \vec{V}_{fk} \quad (22)$$

The relative velocity is determined from Eq. (23) proposed by Manninen et al. [21] while Eq. (24) by Schiller and Naumann [22] is used to calculate the drag function ( $f_{drag}$ ).

$$\vec{V}_{pf} = \frac{\tau_p d_p^2}{18 \mu_f f_{drag}} \frac{(\rho_p - \rho_{eff})}{\rho_p} \vec{a} \quad (23)$$

$$f_{drag} = \begin{cases} 1 + 0.15 \text{Re}_p^{0.687} & \text{Re}_p \leq 1000 \\ 0.0183 \text{Re}_p & \text{Re}_p > 1000 \end{cases} \quad (24)$$

where  $\text{Re}_p = (V_m d_p)/\nu_{eff}$  and  $\vec{a} = \vec{g} - (\vec{V}_m \cdot \nabla) \vec{V}_m$ .

### 2.3.3. Eulerian

In the Eulerian model there are different kinds of coupling between phases. The pressure is shared by all the phases, while separate continuity, momentum, and energy equations are employed for different phases including primary and secondary phases. The volume of each phase is calculated by integrating its volume fraction throughout the domain, while the summation of all the volume fractions is equal to unity. The relevant equations are:

- Conservation of mass

$$\nabla \cdot (\varphi_q \rho_q \vec{V}_q) = 0 \quad (25)$$

where,  $\vec{V}_q = \int_V \varphi_q dV$ , and  $\sum_{q=1}^n \varphi_q = 1$ , and  $q$  indicates the phase.

- Conservation of Momentum ( $q^{\text{th}}$  phase)

$$\nabla \cdot (\varphi_q \rho_q \vec{V} \vec{V}) = -\varphi_q \nabla P + \varphi_q \nabla \cdot (\mu_q \nabla \vec{V}) + \varphi_q \rho_q \vec{g} + \sum_{p=1}^n \vec{R}_{pq} + \vec{F}_{lift,q} \quad (26)$$

where,  $\sum_{p=1}^n \vec{R}_{pq} = \sum_{p=1}^n S_{pq} (\vec{V}_p - \vec{V}_q)$  stands for the interaction forces between the phases,  $S_{pq} = (\varphi_q \varphi_p \rho_q f)/\tau_p$ ,  $\tau_p = (\rho_p d_p^2)/(18 \mu_q)$  and  $f$  indicates the drag friction, which is calculated according to Schiller and Naumann [22] as:

$$f = \frac{C_D \text{Re}}{24} \quad (27)$$

$$C_D = \begin{cases} \frac{24(1 + 0.15 \text{Re}^{0.687})}{\text{Re}} & \text{Re} \leq 1000 \\ 0.44 & \text{Re} > 1000 \end{cases} \quad (28)$$

$$\text{Re} = \frac{\rho_q |\vec{V}_p - \vec{V}_q| d_p}{\mu_q} \quad (29)$$

The lift force is computed from the Drew and Lahey [23] equation:

$$\vec{F}_{lift,q} = -0.5 \rho_p \varphi_q (\vec{V}_p - \vec{V}_q) \times (\nabla \times \vec{V}_q) \quad (30)$$

- Conservation of energy

$$\nabla \cdot (\varphi_q \rho_q \vec{V}_q H_q) = -\nabla \cdot (K_q \nabla T_q) - \tau_q : \nabla \vec{V}_q + \sum_{p=1}^n \vec{Q}_{pq} \quad (31)$$

where,  $\vec{Q}_{pq} = h(\vec{V}_p - \vec{V}_q)$  is the heat exchange coefficient and  $h = (6K_q \varphi_q \varphi_p \text{Nu}_p)/(d_p^2)$ .  $\text{Nu}_p$  is calculated from the Ranz and Marshal [24] model:

$$\text{Nu}_p = 2 + 0.6 \text{Re}^{0.5} \text{Pr}_q^{0.333} \quad (32)$$

where,  $\text{Pr}_q = (C_p \mu_q)/K_q$ .

### 2.4. Boundary conditions

The governing equations for all four approaches have been solved using the following boundary conditions:

- At the tube inlet ( $z = 0$ ):

$$w = V_{in}, u = v = 0, T = T_{in}$$

- At the fluid–solid interface ( $r = D/2$ ):

$$w = u = v = 0, -K_{eff} \left( \frac{\partial T}{\partial r} \right) = q_w$$

- At the tube outlet ( $z = 0.97$ ) all the normal diffusion fluxes are set equal to zero and a mass balance correction is applied.

### 3. Numerical solution

The differential equations were discretized with the control volume technique. For the convective and diffusive terms a second order upwind method was used while the SIMPLEC procedure was employed for the velocity–pressure coupling. Grid independence tests were done separately for each of the four approaches to be sure about the accuracy of results. Many combinations of node numbers in the axial (140, 180, 280), radial (30, 40, 50, 60) and circumferential (32, 40, 48, 60) directions were tested. In all cases the grid is finer close to the wall and the entrance of the tube where the temperature and velocity gradients are large. Typical results are shown in Fig. 2 which illustrates the temperature and velocity profiles calculated with the single phase model at two axial positions ( $Z = 0.2$ ,  $Z = 0.8$ ). They indicate that these particular grid distributions give essentially identical results. Similar results were also obtained for all the two phase models. Following these comparisons the same mesh (180 nodes in the axial direction, 40 nodes in the circumferential direction, and 40 nodes in the radial direction) was chosen for all of four models.

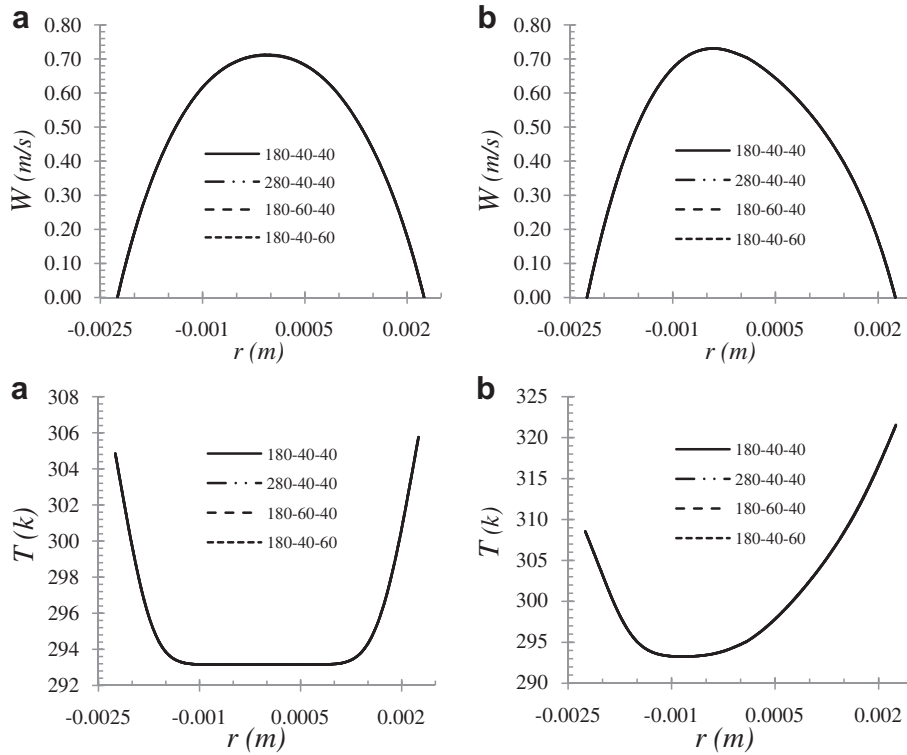


Fig. 2. Model Grid independency test at  $Z = 0.2$  (a) and  $Z = 0.8$  (b).

4. Validation, results and discussion

The previously described geometry and boundary conditions are the same as those of the experimental study by Wen and Ding [14] who measured the fluid inlet and outlet bulk temperatures as well as the wall temperature at five axial positions of the tube, for different mass flow rates and particle volume fractions of a water– $Al_2O_3$  nanofluid. Since, the exact magnitudes of the wall heat flux and inlet temperature are not mentioned in their paper, they were calculated using their axial Nusselt number evolution and the Shah equation [25]. These values were then used to calculate the velocity and temperature distributions in the nanofluid by solving each of the previously described four models. In order to compare these numerical results with the experimental data we then had to evaluate the local convective heat transfer coefficient,  $h(Z)$ . This was done using two different ways of determining the wall temperature from the numerical results. In the first case,  $T_w$  was set equal to the average temperature of all the interfacial nodes. In the second case it was set equal to the average temperature of the nodes in the top half of the interface. Fig. 3 illustrates the differences between the experimental and calculated convective heat transfer coefficients for the single phase model. It shows that, if the wall temperature is calculated as the average of all the interfacial nodes, the convection heat transfer coefficient reaches a constant value after a short distance from the inlet. But, the experimental data shows a continuous change along the entire length of the tube which is similar to the predicted behaviour obtained when the upper half average temperature is used. Similar results were obtained for other particle volume fractions and Reynolds numbers. This result is attributed to the fact that the experimentally determined temperatures were probably measured near the top of the tube which is warmer due to the buoyancy induced temperature stratification in the fluid. Therefore, the average temperature of the upper half of the tube is used to calculate the heat transfer coefficient presented in the following figures.

Figs. 4 and 5 compare the numerical values of the convective heat transfer coefficient predicted by the four models under consideration with the corresponding experimental data for two Reynolds numbers ( $Re = 1050, 1600$  respectively). They clearly show that the single-phase model gives considerably lower estimates than the experimental data for all particle volume fractions and both Reynolds numbers. The predictions of the three two-phase models are essentially identical and closer to the experimental data for practically all axial positions.

Figs. 4 and 5 also show that the convective heat transfer coefficient increases when the particle volume fraction increases. However, the enhancement predicted by the single-phase and two-phase approaches is different and none of them is equal to the corresponding experimental result. For both of the Reynolds numbers the two-phase approach gives closer results to the experimental data; however the possibility of improving the predictions of the single phase model by using different set of correlations for the nanofluid properties can be studied.

The numerical results in Figs. 4 and 5 indicate an average enhancement of the convective heat transfer coefficient by almost 11% when the Reynolds number increases from 1050 to 1600. This

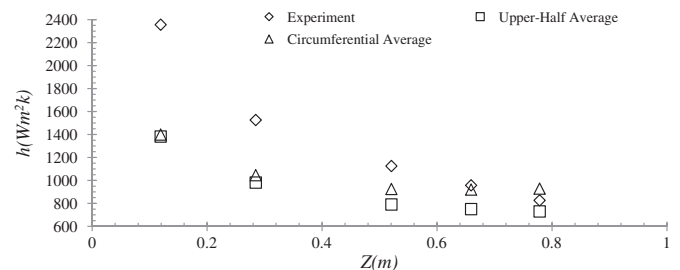


Fig. 3. Convective heat transfer coefficient predicted by the single-phase model with two different determinations of the wall temperature ( $Re = 1600, \phi = 0.006$ ).

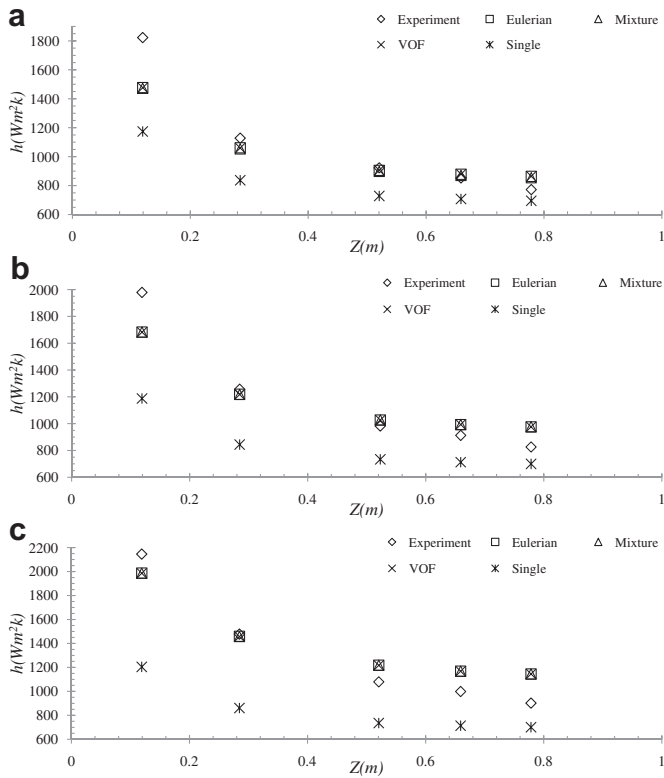


Fig. 4. Comparison of calculated convective heat transfer coefficient with experimental data for  $Re = 1050$  (a:  $\phi = 0.006$ , b:  $\phi = 0.01$ , c:  $\phi = 0.016$ ).

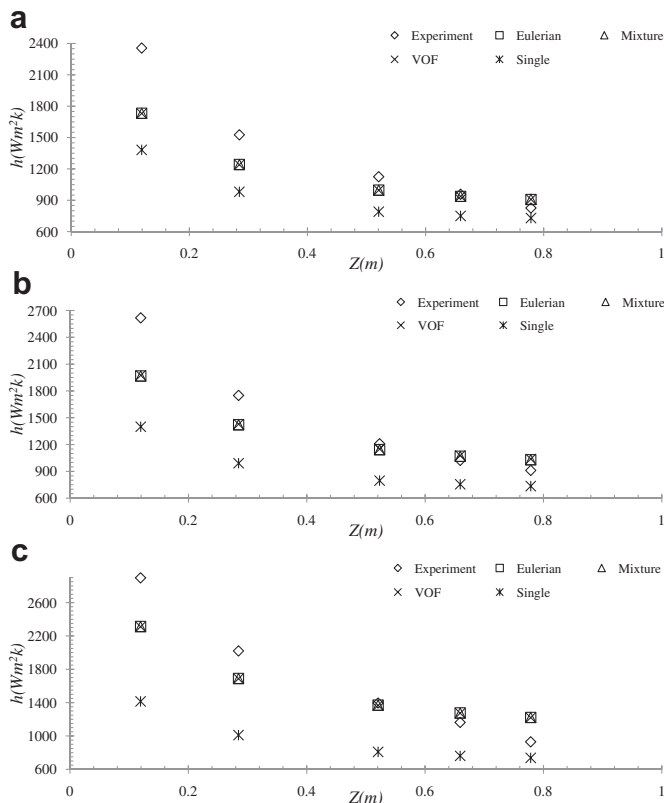


Fig. 5. Comparison of calculated convective heat transfer coefficient with experimental data for  $Re = 1600$  (a:  $\phi = 0.006$ , b:  $\phi = 0.01$ , c:  $\phi = 0.016$ ).

value is the same for single-phase and two-phase models and approximately half of the corresponding value derived from the experimental data.

The effect of nanoparticle volume fraction on the average heat transfer coefficient is illustrated in Fig. 6. It is obvious from these results that the predictions of the single-phase model reflect neither the qualitative nor the quantitative behaviour of the experimental values. The experimental data shows an average enhancement of about 20% and 24% respectively for  $Re = 1050$  and  $Re = 1600$  as the result of a 1% increase in alumina particles volume fraction. For the lower Reynolds number, this is about 11.6 times larger than the corresponding numerical result from the single-phase model and 1.7 times smaller than the two-phase models result, and for the higher Reynolds number about 11.3 times larger than the corresponding numerical result from the single-phase model and 1.5 times smaller than the two-phase models result. On the other hand, the predictions of the two-phase models (all three give essentially identical results as those of the Eulerian model shown in Fig. 6) are in fairly good agreement with the experimental data despite the fact that they indicate a higher enhancement as  $\phi$  increases.

These comparisons of experimental and calculated heat transfer coefficients show some of the differences between results obtained by the models under consideration. Further comparisons of other significant calculated variables are provided in the following paragraphs.

Fig. 7 illustrates the secondary flow velocity vectors and temperature contours in two planes ( $Z = 0.4$  m and  $Z = 0.8$  m) for  $Re = 1050$  and  $\phi = 0.01$ . The temperature contours predicted by all the models are qualitatively similar. They evolve from a quasi-elliptical form at  $Z = 0.4$  m to a kidney form at  $Z = 0.8$  m. However, the maximum values predicted by the single-phase model are significantly higher. On the other hand, the velocity vectors define two symmetrical counter-rotating vortices. They are generated by the density differences between the warm fluid in contact with the wall and the cool fluid situated just below the axis of the tube. The magnitude of the velocity vectors predicted by the single-phase and VOF models is slightly greater than for the corresponding predictions by the Mixture and Eulerian models.

In contrast to the temperature which increases in the axial direction, the corresponding secondary flow velocities are more important at  $Z = 0.4$  m than at  $Z = 0.8$  m. Furthermore, the difference between the highest upward velocity and the highest downward velocity along the horizontal diameter is more important at  $Z = 0.4$  m than at  $Z = 0.8$  m for all models. Similarly, the difference between the highest and lowest temperatures along this same diameter is more important at  $Z = 0.4$  m than at  $Z = 0.8$  m for all models. This is consistent with the results by Ouzzane and Galanis [26] and Orfi et al. [27], who have shown that the buoyancy induced secondary flow is less important in the fully developed region.

In Fig. 8 (higher Reynolds number) the velocity vectors and temperature contours show the same qualitative behaviour as in Fig. 7. However, in contrast to the results of Fig. 7, the secondary flow velocity vectors at  $Z = 0.4$  m are weaker than at  $Z = 0.8$  m. A survey of the results for  $Re = 1600$  indicates that the most important secondary velocity vectors occur at a position further downstream than  $Z = 0.4$  m. This is again consistent with the results by Ouzzane and Galanis [26] and Orfi et al. [27] and can be explained by the fact that the hydrodynamic and thermal development lengths increase with the Reynolds number.

Fig. 9 illustrates the axial velocity profiles along the vertical diameter close to the inlet ( $Z = 0.2$  m) and outlet ( $Z = 0.8$  m) of the tube for a given Reynolds number and volume fraction. The predictions of the two-phase models are essentially identical. Near

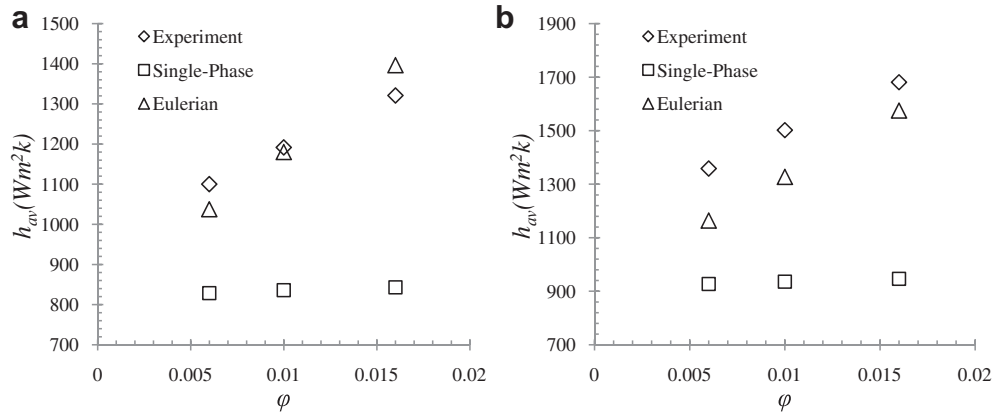


Fig. 6. Average convective heat transfer coefficient (a:  $Re = 1050$ , b:  $Re = 1600$ ).

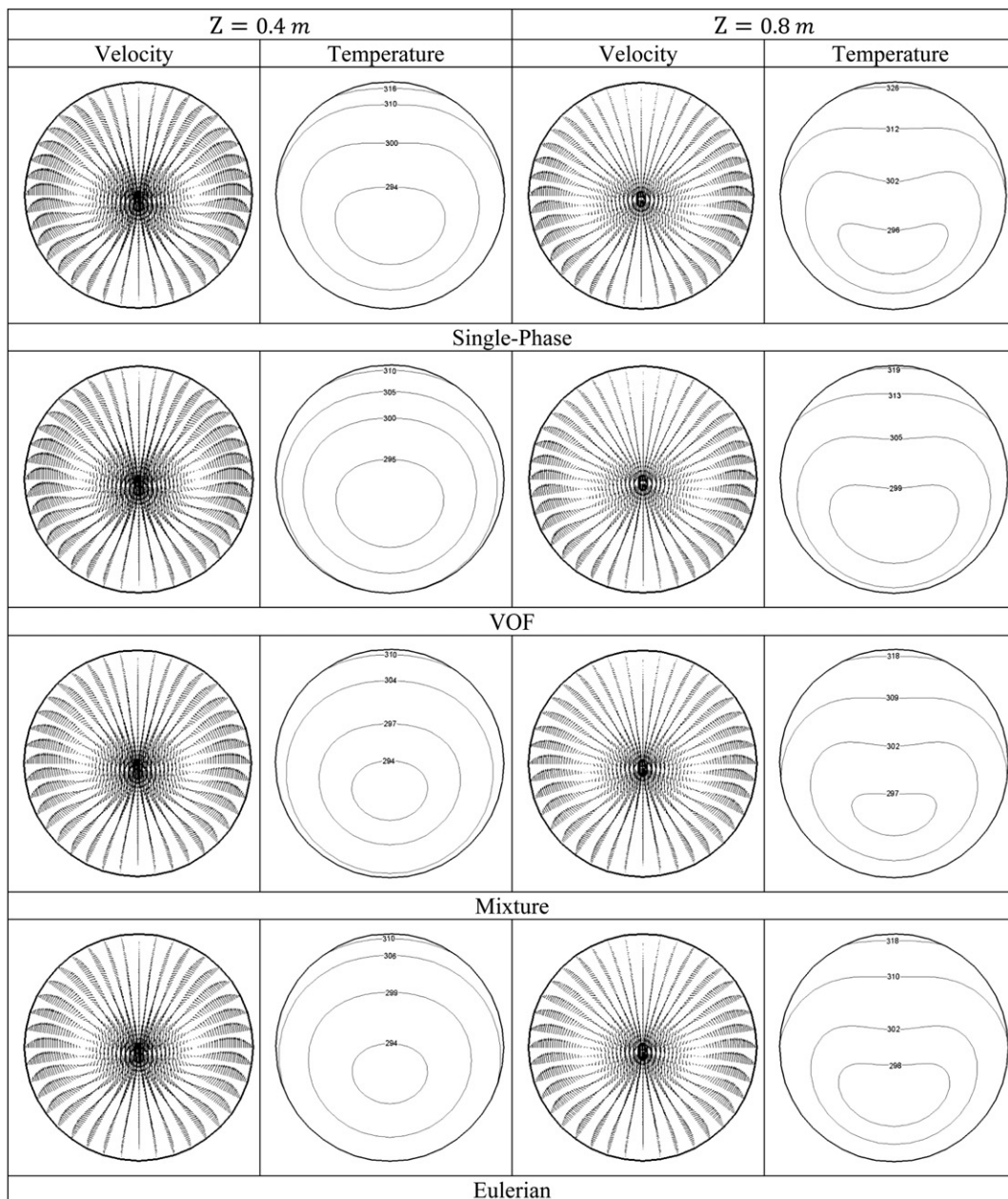


Fig. 7. Secondary flow velocity vectors and temperature contours for  $Re = 1050$ ,  $\phi = 0.01$ .

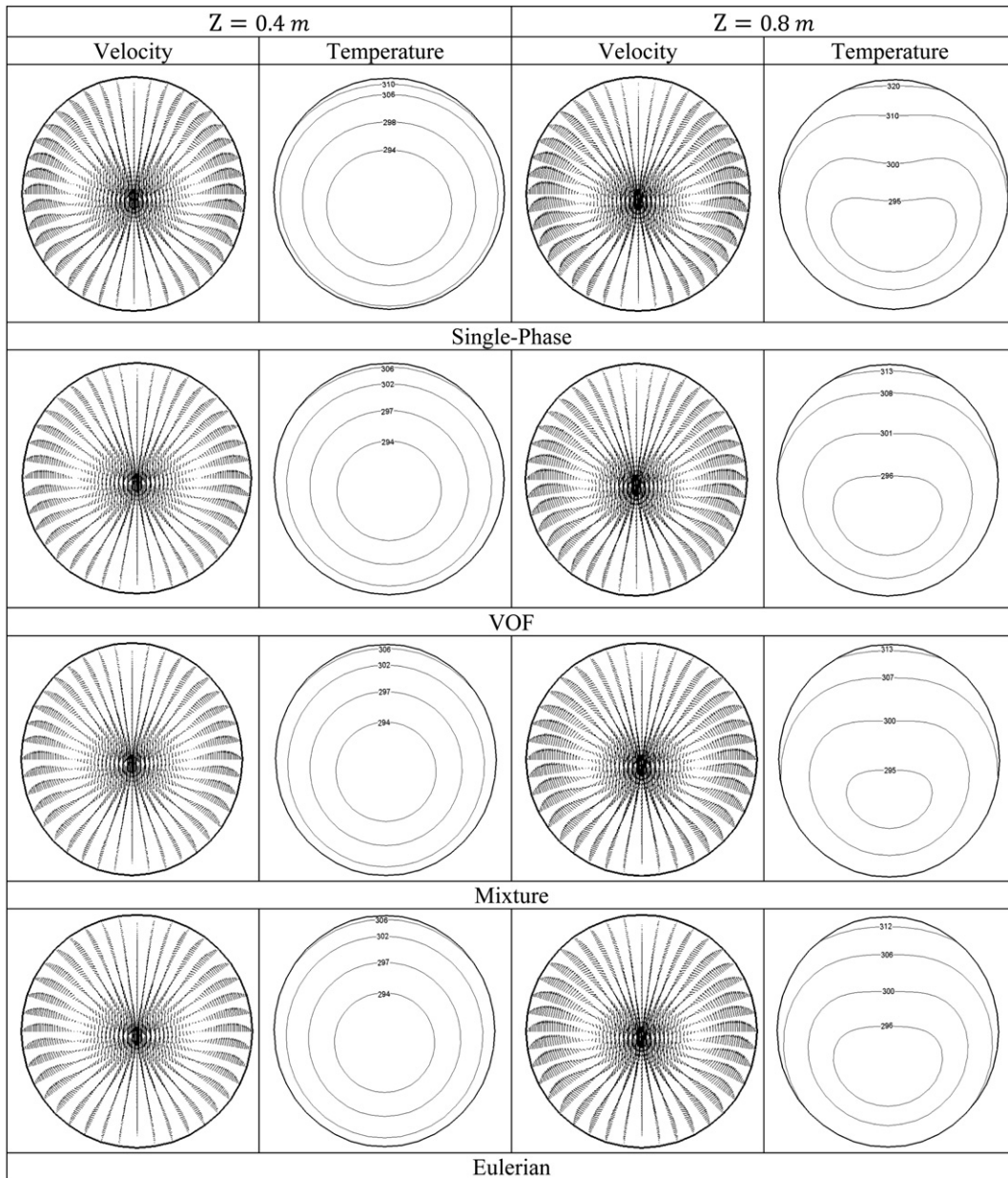


Fig. 8. Secondary flow velocity vectors and temperature contours for  $Re = 1600$ ,  $\phi = 0.01$ .

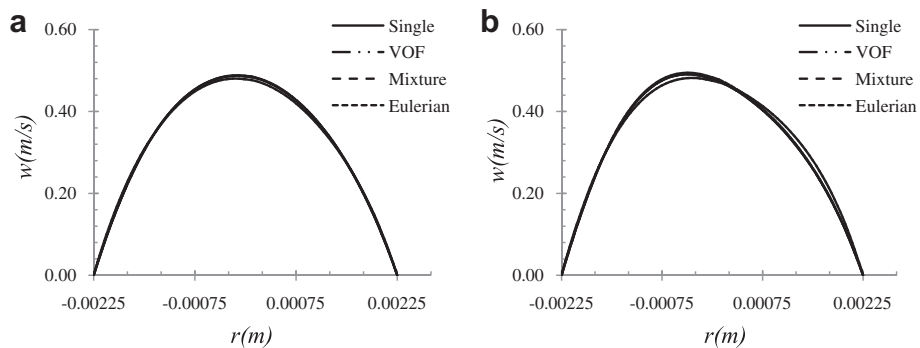


Fig. 9. Axial velocity profiles for  $Re = 1050$  and  $\phi = 0.016$  (a:  $Z = 0.2$  m, b:  $Z = 0.8$  m).

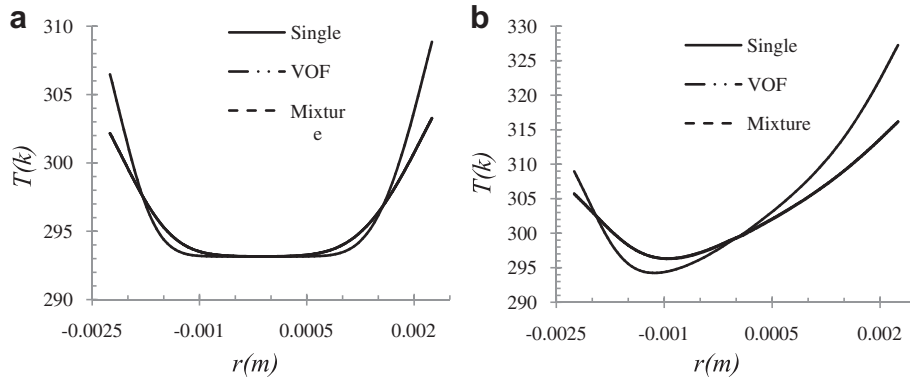


Fig. 10. Temperature profiles for  $Re = 1050$  and  $\varphi = 0.016$  (a:  $Z = 0.2$  m, b:  $Z = 0.8$  m).

the tube’s inlet they are also quite close to the profile predicted by the single-phase model. On the other hand, near the outlet the profiles predicted by the single-phase and two-phase models are somewhat different. The main differences between these velocity profiles are the magnitude and position of the maximum axial velocity. In general, the maximum values predicted by the two-phase models are slightly higher. The difference in the position of this maximum velocity is due to the buoyancy induced secondary movement which was discussed earlier.

Fig. 10 shows the temperature profiles along the vertical diameter for the same conditions as in Fig. 9. All the models indicate that fluid in the top half of the tube is warmer than in the bottom half since warm fluid has a lower density and rises under the influence of buoyancy. This is particularly evident near the outlet of the tube (Fig. 10b). We note that the predictions of all the two-phase models are again essentially the same but, contrary to the results depicted in Fig. 9, the differences from the profiles predicted by the one-phase model are important. Thus, at a given axial position, the difference between the minimum and maximum fluid temperature is considerably higher in the case of the one-phase model. The same is true for the difference between the wall temperature at the bottom ( $r = -0.025$  m) and top ( $r = 0.025$  m) of the tube.

The results of calculations with one-phase and two-phase models shown in Figs. 9 and 10 (as well as those for other axial positions not shown here) clearly indicate that their predictions of the axial velocity are quite similar while those of the temperature distribution are very different.

Figs. 11 and 12 show the axial velocity and temperature profiles along the vertical diameter for a higher Reynolds numbers than in Figs. 9 and 10. The differences between predictions by the single-phase and two-phase models decrease as the Reynolds number increases but they remain significant in the case of temperature profiles (Fig. 12). In addition, the increase of the Reynolds number is accompanied by a decrease of the asymmetry of the velocity and temperature profiles. This effect of the Reynolds number is due to the fact that its increase is accompanied by a decrease of the influence of natural convection and a weakening of the buoyancy induced secondary flow which leads to the accumulation of warm lighter fluid in the upper half of the cross section.

A careful examination of Figs. 9–12 indicates that wherever a particular model predicts higher temperatures it also predicts higher velocities. Thus, close to the walls, where temperatures predicted by the single-phase model are higher, the velocities predicted by the two-phase models are smaller. On the other hand, in the region where the two-phase models predict higher temperatures the velocities predicted by the one-phase model are smaller.

For lower volume fractions the differences between predictions by the one-phase and two-phase models are smaller than those shown in Figs. 9–12. However, they are still significant for temperature profiles, even for very low volume fractions ( $\varphi = 0.006$ ).

Fig. 13 shows the predicted axial evolution of the centerline velocity. It is seen that the predictions of different two-phase models are almost identical while those of the single-phase model

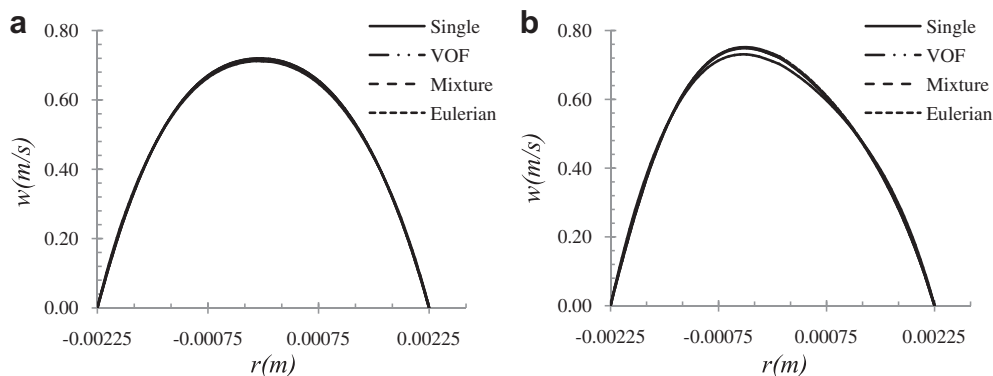


Fig. 11. Axial velocity profiles for  $Re = 1600$  and  $\varphi = 0.016$  (a:  $Z = 0.2$  m, b:  $Z = 0.8$  m).

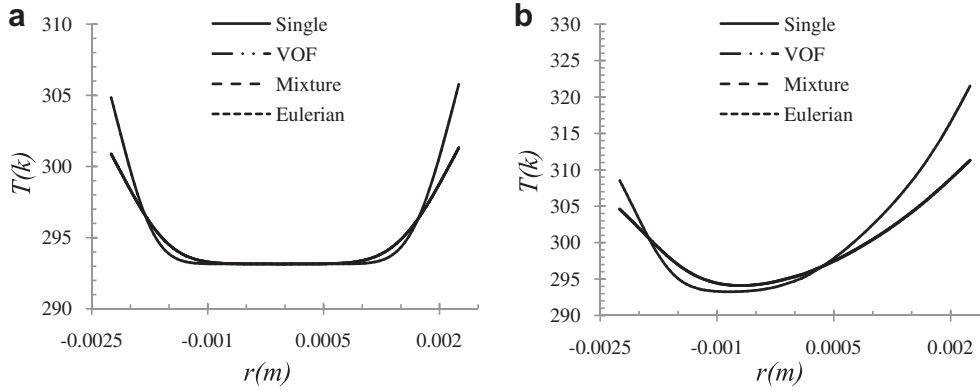


Fig. 12. Temperature profiles for  $Re = 1600$  and  $\phi = 0.016$  (a:  $Z = 0.2$  m, b:  $Z = 0.8$  m).

are always lower than the two-phase estimates. The difference between single- and two-phase results increases for higher particle volume fractions. The magnitude of this velocity initially increases due to the growth of the boundary layer, reaches a maximum and then decreases slightly towards a minimum before attaining an essentially constant value in the hydrodynamically developed region. This behaviour is characteristic of all mixed convection flows [9,26,27] and is due to the buoyancy induced secondary flow. As noted earlier (Figs. 9 and 11) this secondary flow pushes downwards the maximum axial velocity which is slightly greater than that depicted in Fig. 13. The difference between the maximum and minimum centerline velocity is greater for  $Re = 1050$  since in this case the effect of natural convection is more important than for  $Re = 1600$ . For this reason the secondary flow starts to develop earlier for the lower Reynolds number and as a consequence the corresponding minimum and maximum centerline velocities occur closer to the tube inlet in this case. The final increase of the

centerline velocity towards its asymptotic value is due to the weakening of the secondary flow in the downstream region of the tube where the fluid temperature becomes more uniform as illustrated and discussed earlier (Figs. 7 and 8).

Fig. 14 shows the axial evolution of the centerline temperature as predicted by the different models. Similarly to the corresponding velocity results (Fig. 13), the single phase predictions are always lower than the two phase estimations, while those of different two phase models are almost the same. The difference increases for bigger particle volume fraction. The effect of the wall heat flux reaches the tube centerline earlier in the case of the lower Reynolds number. This is due to the secondary flow which close to the tube entrance is stronger for lower Reynolds number.

Fig. 15 compares the calculated skin friction coefficients for a given particle volume fraction and two Reynolds numbers. The lowest results are calculated by the Eulerian two-phase model. The results for the single-phase and the other two-phase models are

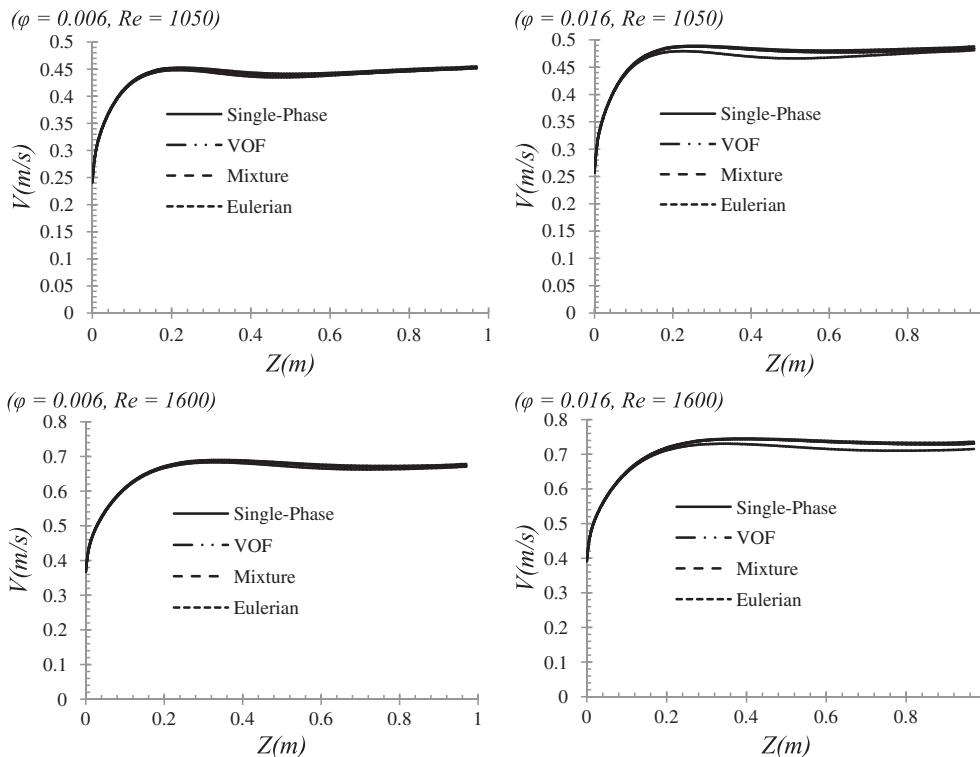


Fig. 13. Axial evolution of centerline velocity.

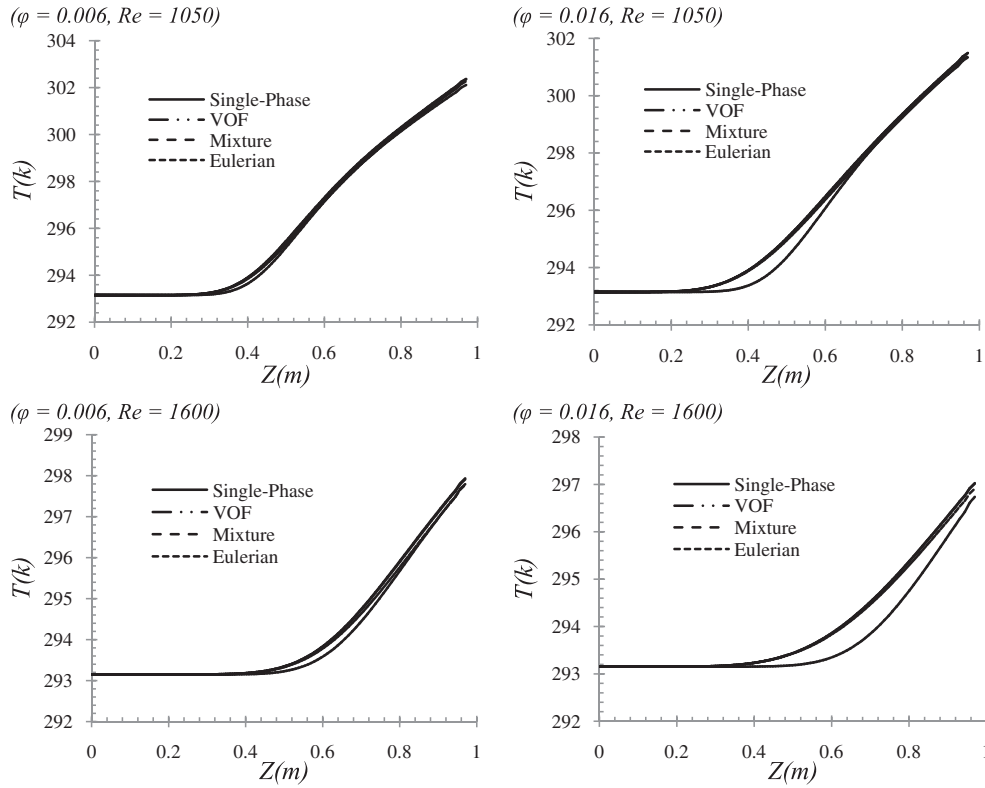


Fig. 14. Axial evolution of centerline temperature.

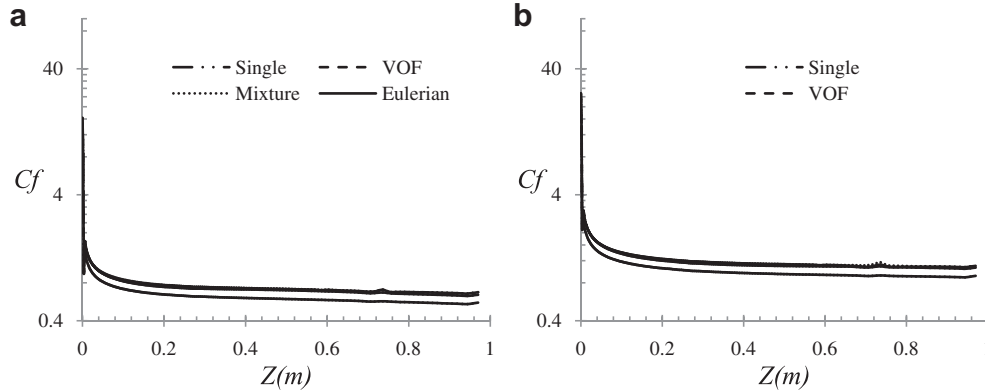


Fig. 15. Axial evolution of the skin friction coefficient for  $\phi = 0.016$  (a:  $Re = 1050$ , b:  $Re = 1600$ ).

quite close although the single-phase model gives somewhat lower estimates. All models show that the skin friction coefficient increases when the Reynolds number increases with approximately the same rate.

### 5. Conclusions

Laminar mixed convection of  $Al_2O_3$ –Water nanofluid inside a horizontal tube was considered. The flow field was predicted numerically using the single-phase and three different two-phase models (VOF, Mixture, and Eulerian). The validity of the calculated results was established by comparing them with existing experimental data for two different Reynolds numbers. The following results were obtained:

- The predictions by the three two-phase models are essentially the same. Therefore, the less expensive model (VOF) is to be preferred for this problem.
- For the problem under consideration the two-phase models give closer predictions of the convective heat transfer coefficient to the experimental data than the single-phase model.
- Nevertheless, the two-phase models over-predict the enhancement of the convective heat transfer coefficient resulting from the increase of the alumina volume fraction.
- Single-phase and two-phase models predict almost identical hydrodynamic fields but very different thermal ones.

It is recommended that these models be compared to other experimental data for different flow conditions to reach a more complete understanding of their ability to predict the nanofluids

thermal and hydrodynamic behaviour. It is also recommended that the effect of using, different combinations of nanofluids property models on the numerical results be evaluated.

### Acknowledgements

This project is part of the R&D program of the NSERC Chair in Industrial Energy Efficiency established in 2006 at Université de Sherbrooke. The authors acknowledge the support of the Natural Sciences & Engineering Research Council of Canada, Hydro Québec, Rio Tinto Alcan and CANMET Energy Technology Center.

### References

- [1] J.C. Maxwell, *Electricity and Magnetism*. Clarendon, Oxford, UK, 1873.
- [2] S.U.S. Choi, Enhancing thermal conductivity of fluids with nanoparticles, November 12–17, in: *Proceedings of the 1995 ASME International Mechanical Engineering Congress and Exposition*, vol. 231. ASME, San Francisco, CA, USA, 1995, pp. 99–105.
- [3] Y. Mori, K. Futagami, S. Tokuda, M. Nakamura, Forced convective heat transfer in uniformly heated horizontal tubes 1st report-experimental study on the effect of buoyancy, *Int. J. Heat Mass Transfer* 9 (1966) 453–463.
- [4] D.P. Siegwarth, T.J. Hanratty, Computational and experimental study of the effect of secondary flow on the temperature field and primary flow in a heated horizontal tube, *Int. J. Heat Mass Transfer* 13 (1970) 27–42.
- [5] S.V. Patankar, S. Ramadhyani, E.M. Sparrow, Effect of circumferentially nonuniform heating on laminar combined convection in a horizontal tube, *J. Heat Transfer* 100 (1978) 63–70.
- [6] K.C. Cheng, F.P. Yuen Presented at the 23rd National Heat Transfer Conference, Flow Visualization Studies on Secondary Flow Pattern for Mixed Convection in the Thermal Entrance Region of Isothermally Heated Inclined Pipes, *Fundamentals of Forced and Mixed Convection*, vol. 42, ASME, Denver, CO, USA, 1985, pp. 121–130.
- [7] C. Zhang, Mixed convection inside horizontal tubes with nominally uniform heat flux, August 9–12, in: *28th National Heat Transfer Conference*, vol. 88, Issue 288, AIChE Symposium Series, San Diego, CA, USA, 1992, pp. 212–219.
- [8] G.J. Hwang, H.C. Lai, Laminar convective heat transfer in a horizontal isothermal tube for high Rayleigh numbers, *Int. J. Heat Mass Transfer* 37 (1994) 1631–1640.
- [9] M. Akbari, A. Behzadmehr, Developing mixed convection of a nanofluid in a horizontal tube with uniform heat flux, *Int. J. Numer. Meth. Heat Fluid Flow* 17 (2007) 566–586.
- [10] M. Akbari, A. Behzadmehr, F. Shahraki, Fully developed mixed convection in horizontal and inclined tubes with uniform heat flux using nanofluid, *Int. J. Heat Fluid Flow* 29 (2008) 545–556.
- [11] S. Mirmasoumi, A. Behzadmehr, Numerical study of laminar mixed convection of a nanofluid in a horizontal tube using two-phase mixture model, *Appl. Therm. Eng.* 28 (2008) 717–727.
- [12] A. Behzadmehr, M. Saffar-Avval, N. Galanis, Prediction of turbulent forced convection of a nanofluid in a tube with uniform heat flux using a two phase approach, *Int. J. Heat Fluid Flow* 28 (2007) 211–219.
- [13] R. Lotfi, Y. Saboohi, A.M. Rashidi, Numerical study of forced convective heat transfer of nanofluids: comparison of different approaches, *Int. Commun. Heat Mass Transfer* 37 (2010) 74–78.
- [14] D. Wen, Y. Ding, Experimental investigation into convective heat transfer of nanofluids at the entrance region under laminar flow conditions, *Int. J. Heat Mass Transfer* 47 (2004) 5181–5188.
- [15] N.B. Vargaftik, *Tables on the Thermophysical Properties of Liquids and Gases*. John Wiley & Sons, New York, 1975.
- [16] C.H. Chon, K.D. Kihm, S.P. Lee, Empirical correlation finding the role of temperature and particle size for nanofluid ( $Al_2O_3$ ) thermal conductivity enhancement, *Appl. Phys. Lett.* 87 (2005) 1–3.
- [17] R.B. Mansour, N. Galanis, C.T. Nguyen, Effect of uncertainties in physical properties on forced convection heat transfer with nanofluids, *Appl. Therm. Eng.* 27 (2007) 240–249.
- [18] K. Khanafer, K. Vafai, M. Lightstone, Buoyancy-driven heat transfer enhancement in a two-dimensional enclosure utilizing nanofluids, *Int. J. Heat Mass Transfer* 46 (2003) 3639–3653.
- [19] S.E.B. Maïga, C.T. Nguyen, N. Galanis, Heat transfer behaviors of nanofluids in a uniformly heated tube, *Superlattice. Microstruct.* 35 (2004) 543–557.
- [20] S.P. Jang, S.U.S. Choi, Effects of various parameters on nanofluid thermal conductivity, *Trans. ASME J. Heat Transfer* 129 (2007) 617–623.
- [21] M. Manninen, V. Taivassalo, S. Kallio, On the Mixture Model for Multiphase Flow. VTT Publications 288, 1996, 3–67.
- [22] L. Schiller, A. Naumann, A drag coefficient correlation, *Z. Ver. Deutsch. Ing.* 77 (1935) 318–320.
- [23] D.A. Drew, R.T. Lahey, *Particulate Two-phase Flow*. Butterworth-Heinemann, Boston, 1993.
- [24] W.E. Ranz, W.R. Marshall, Evaporation from drops, part I, *Chem. Eng. Prog.* 48 (1952) 141–146.
- [25] R.K. Shah, Thermal entry length solutions for the circular tube and parallel plates, 3rd National Heat and Mass Transfer Conference, Indian Institute of Technology, Bombay, 1, 1975, pp. HMT-11–75.
- [26] M. Ouzzane, N. Galanis, Developing mixed convection in an inclined tube with circumferentially nonuniform heating at its outer surface, *Numer. Heat Transfer Part A: Applications* 35 (1999) 609–628.
- [27] J. Orfi, N. Galanis, C.T. Nguyen, Laminar mixed convection in the entrance region of inclined pipes with high uniform heat fluxes, June 21–24, in: *Proceedings of the 1998 ASHRAE Annual Meeting*, vol. 88, Issue 2, ASHRAE Transactions, Toronto, ON, Canada, 1998, pp. 417–428.